# A contribution to variance analysis of 3D-displacement extracted from GB-SAR measurements

**Aiham Hassan[1], Jinjun Xu[2], Cheng Xing[2], Volker Schwieger[1]**

Received: September 2018 / Accepted: Octomber 2018 / Published: March 2019


## Abstract

The Ground-Based Synthetic Aperture RADAR (GB-SAR) is a remote sensing technique, which has been used in the last two decades for many monitoring tasks of both man-made and natural objects. The advantages of GB-SAR are its high temporal and spatial resolution and its high accuracy in detection of displacements in LOS-direction for the whole observed area. The major limitation of GB-SAR is the ability to detect just displacement component in LOS-direction; further displacement components cannot be detected. The common method to overcome this problem is to transform the LOS-displacement into a 3D-coordinate system in which the direction of the real displacement is also defined. For this transformation additional observations are required, which can be observed by means of conventional measurement techniques e.g. GNSS or TLS. The accuracy of the transformed displacement will be affected by the uncertainties of the additional observations. In this study the accuracy of the transformed 3D-displacemnt is investigated using a simulation under four different scenarios for the accuracies of the additional observations. The results of the investigation show high sensitivity of the accuracy to the angle between LOS- and real displacement direction and to the accuracy of the expected real displacement direction. The sensitivity to the accuracy of sensor and pixel position and to the accuracy of the LOS-displacement is very low. The results of the theoretical study are approved through a practical study case.

## Keywords

Engineering survey, GB-SAR, Monitoring, Standard Deviation, Error Propagation, 3D-Displacement.

[1] M.Sc. A. Hassan & Prof. Dr.-Ing. habil. V. Schwieger
Institute of Engineering Geodesy/ Faculty of Aerospace Engineering and Geodesy/ University of Stuttgart
Geschwister-Scholl-Str. 24D, Stuttgart, Germany
E-mail: aiham.hassan@iigs.uni-stuttgart.de

[2] Prof. Dr. J. Xu & Dr. C. Xing
Institute of Surveying Engineering/ School of Geodesy and Geomatics/ Wuhan University
129 Luoyu Road, Wuhan, P. R. China
E-mail: jjxu@sgg.whu.edu.cn

## 1. Introduction

The Ground-Based Synthetic Aperture RADAR (GB-SAR) is a remote sensing technique, which has been used in the last two decades for many monitoring tasks of both man-made and natural objects. The potential of the technique in this field was been approved through many studies e.g. monitoring of landslide movements (Noferini et al., 2007; Herrera et al., 2009; Luzi et al., 2010 ), glacier (Luzi et al., 2007), snow avalanche (Martinez-Vazquez & Fortuny-Guasch, 2008), dam (Xing et. al., 2014). The advantages of GB-SAR are its high temporal and spatial resolution and its high accuracy in detection of displacements in the line of sight (LOS) direction for the whole illuminated area. Measurements are possible independent from day light and almost regardless of weather conditions because of the larger wavelength comparing to other geodetic optical techniques. Monitoring of hazardous areas is possible contactless, which is very important for the safety of the measurement crew.

The accuracy of the LOS-displacement depends on different factors; these will be the subject of section 2. This accuracy is usually in sub-millimeter range, which is much better than the accuracies of conventional geodetic monitoring techniques such as total station, GNSS and Laser scanning. However the LOS-displacement is just a projection of the real displacement on the LOS-direction, and therefore just a part of it which does not give any information about the real direction of the displacement. Additional information are needed in order to get the real displacement from GB-SAR data. These information and the transformation between LOS- and real displacement will be the subject of section 3. The accuracy of the transformed displacement will be affected by the uncertainties of the additional information needed for this transformation. The main focus of this study will be on the investigation of this accuracy under different configuration in order to quantify it and to determine the main influence factors (section 4).

The results of this theoretical investigation will be applied for a practical monitoring task for a landslide in the Three Gorges area in China (section 5).

## 2. Accuracy of LOS-displacement

GB-SAR uses the phase difference i.e. interferometric phase between two SAR images collected from the same sensor position at two different time periods to determine the change of the distance between SAR-sensor and target. Besides of the change of the distance the interferometric phase $\varphi_w$ will be affected by phase shift caused by the atmospheric disturbances $\varphi_{atm}$ and noise $\varphi_{noise}$. So the phase shift caused by actual displacement $\varphi_{disp}$ can be expressed as:

$$\varphi_{disp} = \varphi_w - \varphi_{atm} - \varphi_{nois} + 2\pi N, \quad (1)$$

N is the integer phase ambiguity, which should be determined when a displacement lager than $\frac{\lambda}{4}$ occurs. This operation is named phase unwrapping, where $\lambda$ is the wavelength of the emitted signal.
It is clear from equation (1) that the accuracy of $\varphi_{disp}$ depends on the accuracy of $\varphi_{atm}$ and the measurement noise.
The accuracy of $\varphi_{atm}$ depends on the range between sensor and target and on the correction method used to estimate $\varphi_{atm}$. Rödelsperger gives a summary about different methods to determine the atmospheric phase and there accuracies, for example while using meteorological observations to determine $\varphi_{atm}$ a 1 % standard deviation in the humidity leads at a temperature of 20 °C, humidity of 50 % and pressure of 1013 hPa to a 60 ° standard deviation of $\varphi_{atm}$ (Rödelsperger, 2011).
Noise consists of system noise (thermal noise) and target dependent noise. The last one depends on the geometric and radiometric properties of the illuminated area (shape, material, roughness, cover, etc.). Corner reflectors, which are characterized through there large RADAR Cross Section (RCS) can be used in order to improve the Signal to Noise Ratio (SNR) in specific pixels. However it is complicated to quantify or to model the influence of the noise because of its target and environment dependency.
The LOS-displacement $\Delta_{LOS}$ can be estimated from $\varphi_{disp}$ as following:

$$\Delta_{LOS} = -\frac{\lambda}{4\pi}\varphi_{disp}. \quad (2)$$

Using error propagation law the standard deviation of $\Delta_{LOS}$ can be estimated from the following formula (Rödelsperger, 2011):

$$\sigma_{\Delta_{LOS}} = \frac{\lambda}{4\pi}\sigma_{\varphi_{disp}}, \quad (3)$$

the accuracy of $\Delta_{LOS}$ is related directly to accuracy of $\varphi_{disp}$ and is furthermore proportional to the wavelength. In this study the followed simulation will be done using the technical specification of the instrument IBIS-L, which uses a signal with a wavelength of $\lambda$=17.4 mm. Assuming a standard deviation of 20 ° for the displacement phase the standard deviation for the LOS-displacement will be $\sigma_{\Delta_{LOS}}$ = 0.5 mm (Rödelsperger, 2011). This value will be assumed as constant along the measurement range and used for the further investigations in section 4.

## 3. From LOS- to 3D-displacement

The major limitation of the GB-SAR is the ability to detect displacements just in LOS-direction. The problematic of getting real 3D-displacement form GB-SAR data was the subject of many publications in the recent years. Severin et. al. (2014) applied two GB-SAR system measuring simultaneously in order to get 3D-displacements. The disadvantage of this method is the need of two GB-SAR systems. Crosetto et al. (2014) proposed noninterferometirc amplitude based procedure to estimate 2D-deformations from GB-SAR images and achieved sub cm accuracy. Hu et. al., 2017 adopted the Multiple Aperture interferometry (MAI) which originates from spaceborne SAR to the GB-SAR. In this method the full GB-SAR aperture is divided into forward-looking and backward-looking aperture, the phase difference between the interferograms of both sub-apertures provides information about the displacement perpendicular to the LOS direction. The last two procedures are limited to detection of 2D-displacemnt.
However the common method is to use coordinate transformation to define the LOS-direction i.e. the position of the sensor and the pixel under investigation in a 3D-coordinate system in which the direction of the real displacement is as well defined. In order to get these additional information conventional measurement techniques e.g. GNSS (Hassan et al., 2018) or TLS (Wang and Xing, 2018) can be used and the LOS-displacement can be transformed to the direction of the real displacement.

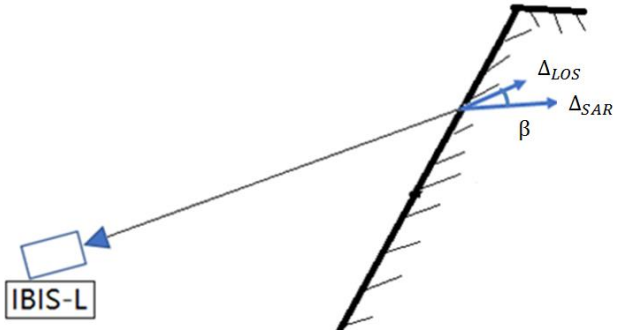


Fig. 15 LOS-displacement and real displacement (Hassan et. al., 2018)

In a 3D-coordinate system (N, E, H) the direction vector of the real displacement can be defined as following:

$$\alpha_{real} = \left(\frac{\Delta N_{real}}{\Delta_{real}}, \frac{\Delta E_{real}}{\Delta_{real}}, \frac{\Delta H_{real}}{\Delta_{real}}\right), \quad (4)$$

where ($\Delta N_{real}$,$\Delta E_{real}$,$\Delta H_{real}$) the North, East and Height components of the real displacement, $\Delta_{real}$ the absolute real displacement:

$$\Delta_{real} = \sqrt{\Delta N_{real}{}^2 + \Delta E_{real}{}^2 + \Delta H_{real}{}^2}\,. \quad (5)$$

The direction vector of the LOS in the same coordinate system is:

$$\alpha_{LOS} = (\frac{N_{SAR}-N_P}{S}, \frac{E_{SAR}-E_P}{S}, \frac{H_{SAR}-H_P}{S}), \quad (6)$$

where ($N_{SAR}$,$E_{SAR}$,$H_{SAR}$) are the coordinates of the SAR sensor, ($N_P$, $E_P$, $H_P$) are the coordinates of the pixel under investigation and S is the slope distance between the sensor and the pixel:

$$S = \sqrt{(N_{SAR} - N_P)^2 + (E_{SAR} - E_P)^2 + (H_{SAR} - H_P)^2}. \quad (7)$$

Using these additional information the angle between LOS-displacement and the real displacement (Fig. 15) could be determined:

$$\cos\beta = \alpha_{LOS} \cdot \alpha_{real}\ , \quad (8)$$

and the LOS-displacement can be transformed to the direction of the real displacement:

$$\Delta_{SAR} = \frac{\Delta_{LOS}}{\cos\beta}\ . \quad (9)$$

## 4. Accuracy of SAR-3D-displacement

The accuracy of $\Delta_{SAR}$ depends on the accuracies of the original observations: ($\Delta N_{real}$, $\Delta E_{real}$, $\Delta H_{real}$, $N_{SAR}$, $E_{SAR}$, $H_{SAR}$, $N_P$, $E_P$, $H_P$, $\Delta_{LOS}$). In order to get this accuracy the equation (9) has been expressed as a function of the original observations:

$$\Delta_{SAR} = f\ (\Delta N_{real}, \Delta E_{real}, \Delta H_{real}, N_{SAR}, E_{SAR}, H_{SAR}, N_P, E_P, H_P, \Delta_{LOS}). \quad (10)$$

This can be done using Matlab symbolic toolbox. The standard deviation of $\Delta_{SAR}$ can be estimated using low of error propagation:

$$\sigma_{\Delta_{SAR}} = \sqrt{F.\Sigma_{ll}.F^T}, \quad (11)$$

where F is the Jacobian matrix of partial derivatives:

$$F = (\frac{\partial\Delta_{SAR}}{\partial\Delta N_{real}}, \frac{\partial\Delta_{SAR}}{\partial\Delta E_{real}}, \ldots., \frac{\partial\Delta_{SAR}}{\partial\Delta_{LOS}}), \quad (12)$$

$\Sigma_{ll}$ is the variance covariance matrix of the observations, it is a diagonal matrix with the variances of the observations on the main diagonal under the assumption of none correlated observations. In order to investigate the main influence factors on the accuracy of $\Delta_{SAR}$ the observations are divided into three groups; the LOS-direction group includes ($N_{SAR}$, $E_{SAR}$, $H_{SAR}$, $N_P$, $E_P$, $H_P$), the real displacement group includes ($\Delta N_{real}$, $\Delta E_{real}$, $\Delta H_{real}$) and the LOS-displacement group includes $\Delta_{LOS}$. Four scenarios are then considered; in each of them the variances of one observation group are changed.

In the first scenario it is assumed that the observations of LOS-direction group are measured using GNSS-RTK and the standard deviations are in cm range. The observations of the real displacement group are measured with GNSS and post processed, consequently their standard deviations are in mm range. The fact that GNSS measuring accuracies for horizontal components are better than those for height components is considered as well for both groups. The standard deviation for the LOS-displacement is assumed to be 0.5 mm.

In fact, the assumption that the accuracies for the observations of the LOS-direction group equal the accuracies for the measurement techniques used for them is not realistic. The reference point of the SAR-sensor is not defined, so the dimensions of the sensor should be considered in the uncertainty of its position. The dimensions of the RADAR-head for the instrument IBIS-L are (27cm, 37.5 cm, 11.5 cm) (IBIS-L v.02.00- User Manual, 2010). Furthermore the exact position of a target or reflecting object within a pixel in the radar image is not exactly defined, so the pixel size should be considered in the uncertainties of its position. The pixel dimension of IBIS-L in the range direction is 0.5 m and in the cross-range direction is 4.4 mrad, which means it depends on the range S between sensor and pixel and can be approximated to 4.4.S in meter units. These dimensions are considered in the accuracies of the LOS-direction group in the second scenario. For each observation in this group the half of the corresponding dimension is assumed as a standard deviation (worst case). The selecting of the corresponding dimension depends on the following assumed measurement configuration, in which the height of the pixel is not affected by its dimension.

In order to investigate the influence of the uncertainties of real displacement direction and LOS-displacement on the result, their uncertainties are changed in scenario 4 and 5 respectively. The assumed standard deviations in each scenario are summarized in Table 1.

For simplification the measurement configuration is assumed as following: SAR-Sensor is horizontally installed and has the coordinate (0 m, 0 m, 100 m) in the 3D-coordinate system (N, E, H). The illuminated area is as well horizontal at the same level of the instrument and practically limited to the range 10 to 1000 m in range direction and to $\pm 55°$ around the mean LOS in the cross range direction. Under this assumption the energy will be scattered back to the sensor only from pixels equipped with a corner reflector. This area is divided in pixels with the size 0.5 m x

Table 1 Standard deviations for the observations in different scenarios

| scenario | $\sigma_{\Delta N_{real}}$ [mm] | $\sigma_{\Delta E_{real}}$ [mm] | $\sigma_{\Delta H_{real}}$ [mm] | $\sigma_{N_{SAR}}$ [mm] | $\sigma_{E_{SAR}}$ [mm] | $\sigma_{H_{SAR}}$ [mm] | $\sigma_{N_P}$ [mm] | $\sigma_{E_P}$ [mm] | $\sigma_{H_P}$ [mm] | $\sigma_{\Delta_{LOS}}$ [mm] |
|---|---|---|---|---|---|---|---|---|---|---|
| 1 | 3 | 3 | 5 | 10 | 10 | 20 | 10 | 10 | 20 | 0.5 |
| 2 | 3 | 3 | 5 | 140 | 190 | 60 | 250 | 4.4.S | 20 | 0.5 |
| 3 | 6 | 6 | 10 | 10 | 10 | 20 | 10 | 10 | 20 | 0.5 |
| 4 | 3 | 3 | 5 | 10 | 10 | 20 | 10 | 10 | 20 | 1 |

4.4 mrad equals the resolution of the instrument IBIS-L in both directions. A horizontal real displacement with the components (-0.1 m, 0 m, 0 m) in the same coordinate system is assumed for the whole illuminated area. The measurement configuration and the results for the first scenario are shown in Fig. 16. To achieve more clarity the pixels and the real displacement are represented larger than their actual dimensions. The detected LOS-displacement in this case varies from -10 cm at the main LOS to -6 cm at the side LOS (Fig. 17).

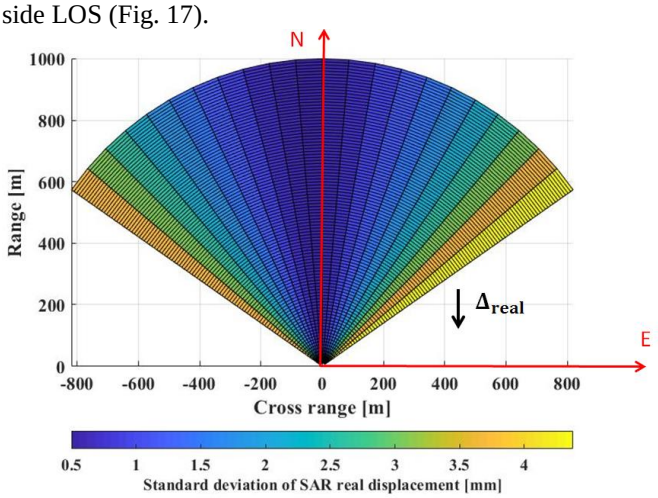


Fig. 16 Simulated Measurement configuration

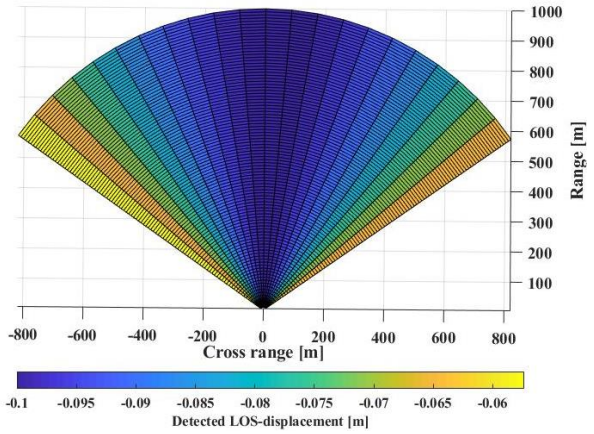


Fig. 17 Detected LOS-displacement for the simulation case

For the above mentioned simulation the angle β increases with the increased cross range but it still limited to the value range for the field of view of the sensor [-55°, +55°], practically further values for this angle are also possible. In order to cover almost any possible situation for this angle the range has been extended to [-80°, +80°]. The values between 80° and 90° are not included due to the fact that interferometric GB-SAR is not sensitive to displacements perpendicular to the LOS. The extended angle range can be simulated either by changing the values of the horizontal components of the simulated real displacement or by extending the field of view for the sensor to ±80°. Even though the last one is just a theoretical assumption and practically impossible, it leads to the same results of the practically possible case and is simpler for the simulation. The results for the first and second scenarios under the extended angle range are shown in Fig. 18 and Fig. 19 respectively.

The results of the first scenario (Fig. 18) clear the importance of the angle β for the result. While the standard deviation of the real SAR displacement at $\beta \in [-10°, 10°]$ remains in sub mm range and so in same range as that for LOS-displacement, increases this standard deviation with increasing angle and reaches the cm range at β = 75°. The maximum standard deviation reaches a value of 17.3 mm at β = 80°. Furthermore the accuracy of the real SAR displacement is range independent in this scenario. This is just valid for the assumption, that the accuracy of the LOS-displacement is range independent as well.

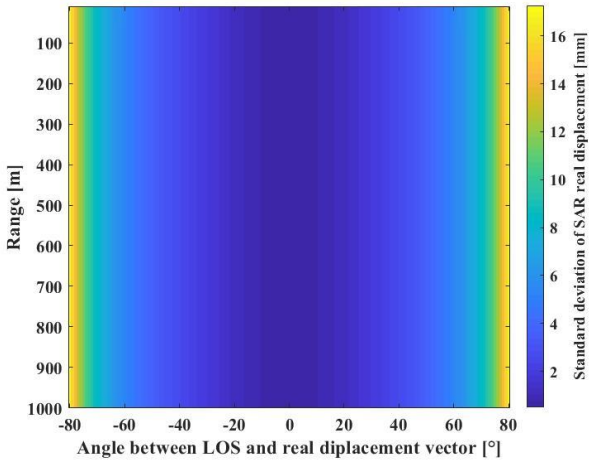


Fig. 18 Standard deviation of the real SAR-displacement for the first scenario

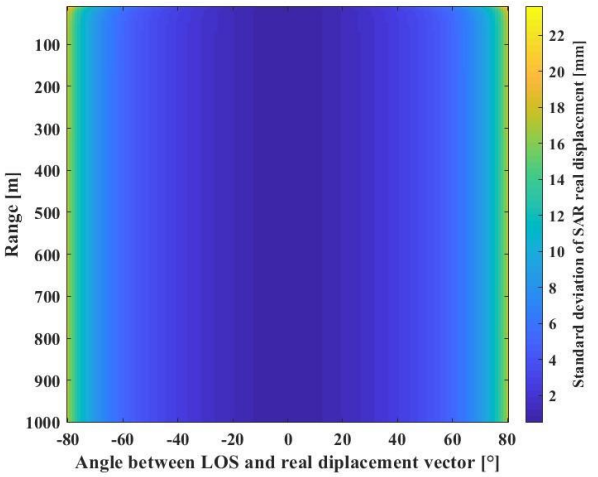


Fig. 19 Standard deviation of the real SAR-displacement for the second scenario

Even for a strong increase of the standard deviations for the observations of the LOS direction group in the second scenario, compared to those in the first scenario, just a slight increase of $\sigma_{\Delta_{SAR}}$ in the close range area and at large values for β with a maximum standard deviation of 23.6 mm in the upper corners of Fig. 19 can be noticed.

To clarify this effect $\sigma_{\Delta_{SAR}}$ for the whole range is

represented in Fig. 20 for three different β angles. Outside the close range area (10 to 100 m range) $\sigma_{\Delta_{SAR}}$ equals that of the first scenario. It increases rapidly in the close range and for large β values. The reason for this increase in the close range is that, the uncertainties in the coordinates of sensor and pixel cause high uncertainties for short distance between sensor and pixel in the LOS-direction vector and thus in the angle β. For the same reason, the increase of the uncertainties of the pixel coordinates with the range cause no noticeable effect.

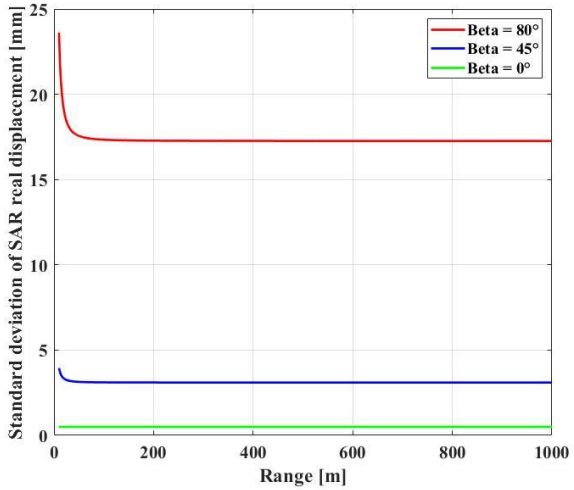


Fig. 20 Standard deviation of the real SAR-displacement for the second scenario along the whole range and under different β angles

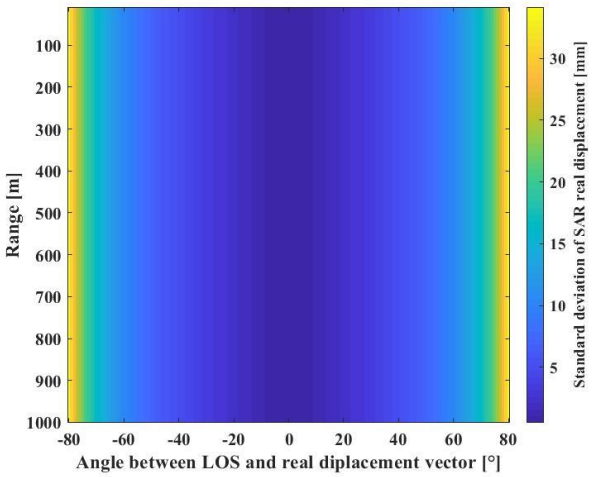


Fig. 21 Standard deviation of the real SAR-displacement for the third scenario

For the same reason and due to the fact that the distance between sensor and pixel is much longer than the real displacement vector, the standard deviation of $\Delta_{SAR}$ is more sensitive for a small change of the uncertainties of the observations in the real displacement group (third scenario), comparing to a large change of the uncertainties of the LOS-direction group (second scenario). The results for the third scenario (Fig. 21) show a similar behaviour as the first scenario (range independent and strong dependent on the angle β). The increase of the standard deviations of the real displacement observation group leads to proportional increase of $\sigma_{\Delta_{SAR}}$. This reaches a maximum value of 34.2 mm for β=80° in the third scenario, which is almost two times the maximum standard deviation in the first scenario, i.e. the same factor as the factor used for increase the standard deviations of the real displacement observation group.

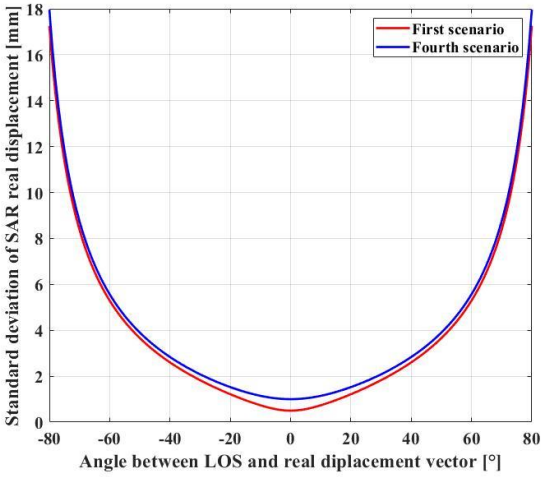


Fig. 22 Standard deviation of the real SAR-displacement for the first and the fourth scenario at 500 m range

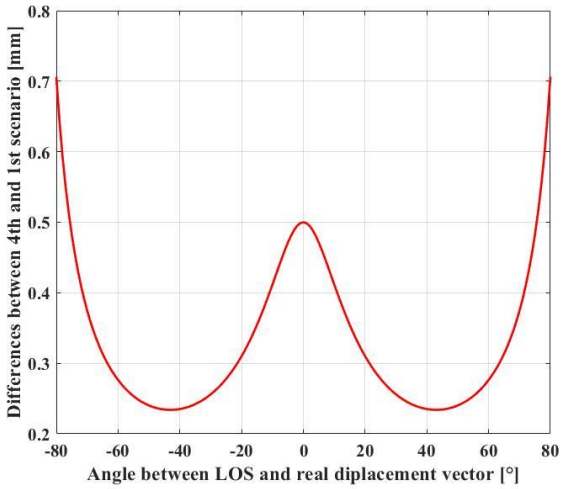


Fig. 23 Differences between $\boldsymbol{\sigma_{\Delta_{SAR}}}$ in the first and fourth scenario

Because of the range independency for $\sigma_{\Delta_{SAR}}$, the results for the fourth scenario are represented at a fix range of 500 m in Fig. 22. To quantify the effect of $\sigma_{\Delta_{LOS}}$ the results of the first scenario are represented in the same figure, and the differences between the standard deviations of $\Delta_{SAR}$ in both scenarios are represented in Fig. 23. A 0.5 mm change in $\sigma_{\Delta_{LOS}}$ at an angle β = 0° leads to an equal change in $\sigma_{\Delta_{SAR}}$. The effect of the same change in $\sigma_{\Delta_{LOS}}$ decreases with increased β and reaches a minimum of 0.22 mm (almost 50% from the original change value) at β = 43°. After that it increases with increased β and reaches a maximum of 0.7

mm at β = 80°.
Considering the results of all scenarios, the angle β is the main influence factor on the accuracy of the real SAR displacement ($\sigma_{\Delta_{SAR}}$), for this reason it is recommended to plan the measurement configuration in the way that, the direction of the sensor main LOS coincide with direction of the expected displacement. The last one can be estimated using further measurements techniques or assumed based on geological or constructive models. Just in this case accuracy for real displacement in the low mm range can be achieved from GB-SAR measurements. The second important factor is the accuracy for the direction of the real displacement. Compared to both factors mentioned above the accuracies of the observations of the LOS-direction and of the LOS-displacement are negligible. Finally it should be mentioned that $\sigma_{\Delta_{SAR}}$ depends also on the value of the measured LOS-displacement, this effect is not been quantified in this simulation.

## 5. Practical case: Lianziya landslide in China

The results of the theoretical variance analysis are applied to a practical monitoring task. The site being monitored is Lianziya landslide, which is located on the south west side of the Yangtze River in the three gorges area in China, more details about this landslide can be found in Hassan et al. (2018). In order to insure the safety of the shipping on the river and of people living in the surrounding towns the landslide was subject of many monitoring campaigns in recent years. A recent one was performed from January 2015 to May 2018 using theodolite measurement system and discovered a horizontal displacement in the north-east direction (to the river). The results of this campaign will be used in this paper to define the direction of the real displacement.
For the monitoring of the landslide using GB-SAR the sensor was installed in a stable area 700 m away from the center of the landslide. Two corner cubes (P1 and P2) were installed within the landslide near a monitoring point from the former campaign mentioned above, the measured displacements at this point was (13.2 mm, 4.3 mm) in North and East direction respectively. The position of the sensor and two corner reflectors were measured using GNSS in order to define the direction of the LOS for both reflectors in the same coordinate system as the one for the real displacement direction. The measurement configuration and the direction of the expected displacement are described in Fig. 24. In this configuration the angles between the real displacement and both LOSs are determined to $\beta_1 = 64.5382°$ and $\beta_2 = 70.5367°$.
The GB-SAR measurements were carried out from 09.03.2018 at 15:52 o'clock to 11.03.2018 at 07:23 o'clock. The atmospheric phase correction was done by means of stable ground control points (GCP) and after that the LOS-displacement time series for P1 and P2 were computed (Fig. 25). Actually within the measurement period of less than 40 hours and taking into account the results of the former monitoring campaign over more than 3 years, the landslide can be considered as stable during the GB-SAR measurement and the LOS-displacement time series in Fig. 25 are caused by errors of atmospheric correction and by noise. The mean values, empirical standard deviation (STD) and root mean square values (RMS) for these time series are calculated and summarized in Table 2.
The RMS values are at the same level as the accuracy for the LOS-displacement proposed in (section 2). These values will be used for the following error propagation.

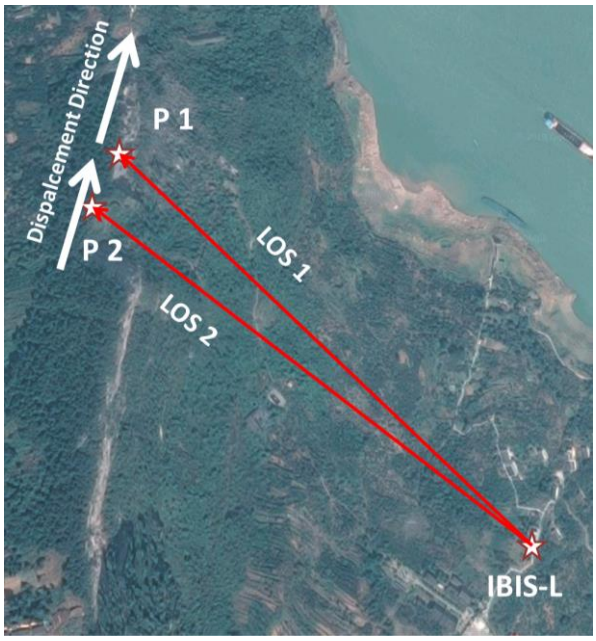


Fig. 24 Measurement configuration and the direction of the expected displacement

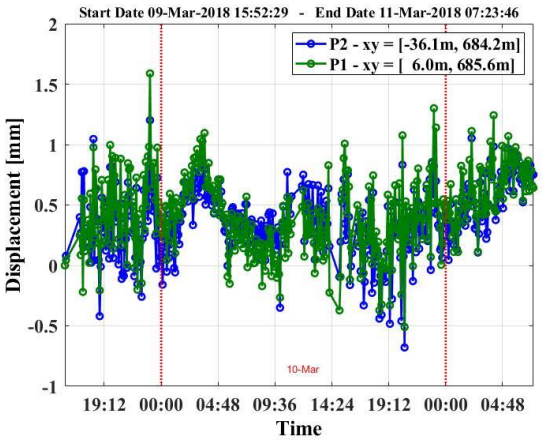


Fig. 25 LOS-displacement time series for P1 and P2

Table 2 Statistics for LOS-displacement time series

| Time series | Mean [mm] | STD [mm] | RMS [mm] | Outlier Per. [%] |
|---|---|---|---|---|
| P1 | 0.42 | 0.32 | 0.54 | 3.9 |
| P2 | 0.37 | 0.28 | 0.47 | 1.5 |

The outliers in both time series are identified using data snooping algorithm and eliminated. The percentages of

these outliers are summarized in Table 2.
Using equation (9) the real SAR-displacement time series for both pixels are computed and represented in figure Fig. 26.
The transformation scales the displacement and the noise depending on the value of β angle. Because of the worst configuration for P2 and in contrast to the LOS-time series the mean values, empirical standard deviations and RMS values for P2 are larger than those for P1. These values are summarized for both real displacement time series in Table 3.

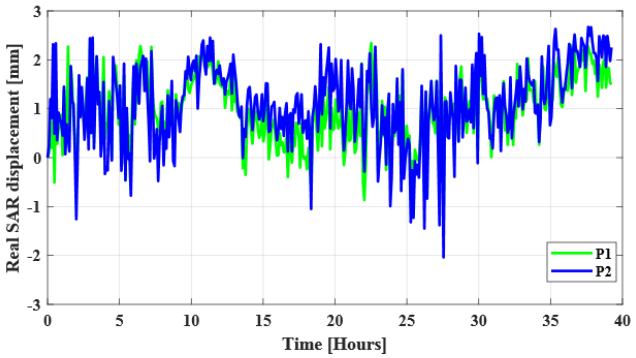


Fig. 26 Real-displacement time series for P1 and P2

Additionally and based on the accuracies of the input observations proposed in the second scenario (Table 1) and on the mean values of the observed LOS-displacement time series (Table 2) the theoretical standard deviations σ for real displacement time series are also calculated (Table 3).

Table 3 Statistics for real-displacement time series

| Time series | Mean [mm] | STD [mm] | RMS [mm] | σ [mm] |
|---|---|---|---|---|
| P1 | 0.98 | 0.70 | 1.20 | 1.39 |
| P2 | 1.10 | 0.82 | 1.37 | 1.66 |

The theoretical standard deviations are in the same level as the empirical RMS values for both pixels. The reason for the differences between these standard deviations and those from the simulation (section 4) under the same configuration is that the measured LOS-displacements in this section are too small compared to the simulated one in the former section.

## 6. Conclusions

GB-SAR is very accurate measurement technique for detection of LOS-displacement. The accuracy of this displacement is usually in sub mm range and depends on the efficiency of the correction method used for atmospheric phase determination and on all kinds of measurement noise. In order to get real 3D-displacement from LOS-displacement a coordinate transformation can be used. For this transformation the position of the sensor, the position of the pixel under investigation and the direction of the real displacement should be determined in the same 3D-coordinate system. The accuracy of the estimated real displacement depends on the accuracies of these additional information and on the measurement configuration, especially the angle β between the LOS-direction and the direction of the real displacement. The last one is the most important factor. While this accuracy is equal to the one of the LOS-displacement (0.5 mm in this study) at β=0°, it get worst with increasing β and reaches in this study a value of 2 cm at β=80°. For this reason it is very important to plan the measurement configuration carefully in order to get reliable results for the real displacement from GB-SAR measurements. The accuracy of the estimated real displacement is also very sensitive to the accuracy of the expected displacement direction, which can be either measured by other measurement techniques or determined based on geological or constructive models, and less sensitive to the accuracies of sensor and pixel positions.

## Acknowledgement

The investigations published in this article are granted by the DAAD (German Academic Exchange Service) project Nr. 5731774 and CSC (China Scholarship Council) within PPP (Project Based Personnel Exchange Program). Therefore the authors cordially thank the funding agencies.

## References

[1] Crosetto, M., Monserrat, O., Luzi, G., Cuevas-González, M., & Devanthéry, N., A noninterferometric procedure for deformation measurement using GB-SAR imagery, IEEE Geoscience and Remote Sensing Letters, 11(1), pp. 34-38, jan. 2014
[2] Hassan, A., Xu, J., Zhang, L., Liu, G., Schmitt, A., Xing, C., Xu, Y., Ouyang, C., & Schwieger, V., Towardes integration of GNSS and GB-SAR measurements: Exemplary monitoring of a rock fall at the Yangtze River in China, FIG kongress, Istanbul, 2018.
[3] Herrera, G., Fernández-Merodo, J. A., Mulas, J., Pastor, M., Luzi, G., & Monserrat, O., A landslide forecasting model using ground based SAR data: The Portalet case study, Engineering Geology, 105(3-4), pp. 220-230, 2009.
[4] Hu, C., Deng, Y., Wang, R., Tian, W., & Zeng, T., Two-dimensional deformation measurement based on multiple aperture interferometry in GB-SAR. IEEE Geoscience and Remote Sensing Letters, 14(2), pp. 208-212, 2017.
[5] IDS, IBIS-L v.02.00- User Manual, Pisa, 2010, (https://fccid.io/UFW-IBIS-LS/User-Manual/User-Manual-1299773), last access 27.08.2018.
[6] Luzi, G., Pieraccini, M., Mecatti, D., Noferini, L., Macaluso, G., Tamburini, A., & Atzeni, C., Monitoring of an alpine glacier by means of ground-based SAR interferometry, IEEE Geoscience and Remote Sensing Letters, 4(3), pp. 495-499, 2007.
[7] Luzi, G., Monserrat, O., Crosetto, M., Copons, R., & Altimir, J., Ground-based SAR interferometry applied to landslide monitoring in mountainous areas. In Mountain

Risks conference: Bringing Science to Society, Firenze (IT), pp. 24-26, 2010.

[8] Martinez-Vazquez, A., & Fortuny-Guasch, J., A GB-SAR processor for snow avalanche identification, IEEE Transactions on Geoscience and Remote Sensing, 46(11), pp. 3948-3956, 2008.

[9] Noferini, L., Pieraccini, M., Mecatti, D., Macaluso, G., Atzeni, C., Mantovani, M., Marcato, G., Pasuto, A., Silvano, S. & Tagliavini, F., Using GB-SAR technique to monitor slow moving landslide, Engineering Geology, 95(3-4), pp. 88-98, 2007.

[10] Rödelsperger, S., Real-time processing of ground based synthetic aperture radar (GB-SAR) measurements (No. 33), PhD thesis, Technische Universität Darmstadt, Fachbereich Bauingenieurwesen und Geodäsie, 2011.

[11] Severin, J., Eberhardt, E., Leoni, L., & Fortin, S., Development and application of a pseudo-3D pit slope displacement map derived from ground-based radar, Engineering Geology, 181, pp. 202-211, 2014.

[12] Wang, P., & Xing, C., Research on coordinate transformation method of GB-SAR image supported by 3D Laser scanning technology, International Archives of the Photogrammetry, Remote Sensing & Spatial Information Sciences, 42(3), 2018.

[13] Xing, C., Huang, J. J., & Han, X. Q., Research on the environmental effects of GB-SAR for dam monitoring. In Advanced Materials Research, Vol. 919, pp. 392-397, Trans Tech Publications, 2014.